Whisker stimulation reinforces a resting-state network in the barrel cortex: nested oscillations and avalanches

Benedetta Mariani[1], Ramón Guevara[1,2], Mattia Tambaro[3,4], Marta Maschietto[4], Alessandro Leparulo[5], Stefano Vassanelli[4,*], Samir Suweis[1,2,*]

1 Padova Neuroscience Center, University of Padova, Italy
2 Department of Physics and Astronomy, University of Padova, Italy
3 Department of Physics, University of Milano Bicocca, Italy
4 Department of Biomedical Sciences, University of Padova, Italy
5 Department of Neuroscience, University of Padova, Italy

*** corresponding authors**

Abstract

The cerebral cortex operates in a state of restless activity, even in the absence of external stimuli. Collective neuronal activities, such as neural avalanches and synchronized oscillations, are also found under rest conditions, and these features have been suggested to support sensory processing, brain readiness for rapid responses, and computational efficiency. The rat barrel cortex and thalamus circuit, with its somatotopic organization for processing whisker movements, provides a powerful system to explore such interplay. To characterize these resting state circuits, we perform simultaneous multi-electrode recordings in rats' barrel cortex and thalamus. During spontaneous activity, oscillations with frequencies centered around 11.5 Hz are detected concomitantly with slow oscillations below 4 Hz, as well as power-law distributed avalanches. The phase of the lower-frequency oscillation appears to modulate the higher-frequency amplitude, and it has a role in gating avalanche occurrences. We then record neural activity during controlled whisker movements to confirm that the 11.5 Hz barrel circuit active at rest is indeed the one involved in response to whisker stimulation. We finally show how a thalamic-driven firing-rate model can describe the entire phenomenology observed at resting state and predict the response of the barrel cortex to controlled whisker movement.

Introduction

The cerebral cortex exhibits a rich repertoire of dynamical states, even in the absence of external stimuli [11, 23, 53, 56, 64]. This continuous and spontaneous activity, known as the resting state, consumes a large portion of the brain's metabolic energy [73], so it is likely to be functional [27]. Indeed, despite the lack of immediate tasks and demands, the resting state is far from idle; instead, it engages various intrinsic circuits, which are thought to serve a range of preparatory and regulatory functions [62]. These resting-state circuits may support the readiness for sensory processing and prepare the brain for rapid responses, effectively setting the stage for context-dependent behaviors [29, 41, 48]. In the cortex, certain networks that activate during rest can also show increased activity when relevant external input arrives, suggesting that these circuits reflect an ongoing state of preparation and prediction, potentially optimized for

varied functional needs of the brain [71]. Interestingly, the diversity of cortical activity at rest is consistent with a system operating near a critical point, where a balance is struck between order and disorder [8, 9, 44] and/or excitation and inhibition [1, 3, 52], allowing various collective patterns to emerge [2, 9, 44]. Neural dynamics in the cortex is often characterized by two main emergent phenomena: neural avalanches and collective sustained oscillations. Neural avalanches are spontaneous cascades of neural activity that propagate through the network, displaying a scale-free distribution—meaning avalanches of all sizes, from small, localized events to large, network-spanning cascades, are observed [3, 20, 24, 26, 38, 46]. Neural oscillations, on the other hand, are rhythmic patterns of activity across different frequency bands (e.g., theta, alpha, gamma) [35, 61] that support the coordination and synchronization of neural populations [6, 7, 21, 31]. These oscillations provide a temporal framework that structures neural activity, organizing the timing of communication across different regions of the cortex [5, 25, 37]. Research has shown that these oscillations can modulate the occurrence and structure of neural avalanches, especially through cross-frequency coupling mechanisms such as theta-gamma coupling [26]. The somatotopic organization of the rat thalamus-barrel circuit for processing whisker movements provides a powerful model to explore this interplay.

By moving the whiskers back and forth, a process called whisking, rats can perceive the shape, size, and texture of nearby objects [16, 72]. This information is encoded into neural impulses and passed through the thalamus to various areas in the sensory-motor cortex [34], most importantly to barrels, located in the primary somatosensory cortex [47, 75], which have a somatotopic correspondence with the whisker on the rat's snout. Furthermore, studies of whisker-related processing have shown that oscillatory activity in the barrel cortex may be closely tied to whisker movements, including both voluntary whisking during exploration and spontaneous twitching during rest [33, 58].

For these reasons, the rat barrel cortex provides an ideal model for studying intrinsic resting-state dynamics and investigating whether it is functionally connected to whisker-related sensory response processing. Importantly for the current work, the hypothesis that circuits that are active at rest could enhance information processing and functional efficiency remains a largely theoretical proposition. Specifically, there is a lack of experimental evidence showing that spontaneous neural activity in cortical circuits is linked to specific functional tasks, such as whisker twitching in the barrel cortex. A possible way to test such a hypothesis is to show that the collective dynamics at rest (e.g., synchronized oscillations) is reinforced during task-related neural processing, such as actual whisker movement. To this end, we analyzed local field potential (LFP) and multi-units activity (MUAs) data recorded from the barrel cortex and thalamus of anesthetized rats (see Figure 1), both during spontaneous activity and after controlled whisker stimulation. An exploratory time-frequency analysis after whisker stimulation averaged over all the trials highlighted two main frequencies: a slow oscillation with frequencies < 4 Hz and an oscillation with frequencies around 11 Hz (Figure 1 (c)) [13, 18, 33, 63, 69]. We studied the frequency content of the signal using the empirical mode decomposition method (EMD), which allows us to perform a systematic frequency decomposition of the LFPs signals [30]. We then exploited MUAs to study avalanches. We showed that neural oscillations (in the 7.5–15 Hz range) and neural avalanches are functionally coupled in the rat barrel cortex and may work together to support whisker-related processing, even in the absence of direct stimulation. To substantiate such a hypothesis, we also recorded neural activity during controlled whisker movements and showed that the frequency centered around 11.5 Hz is strongly reinforced in the barrel cortex as a response to whisker stimulation. We finally show how a thalamic-driven firing model [50] can describe the entire phenomenology observed at resting state and predict the response of the barrel cortex in the controlled whisker

movement experiments.

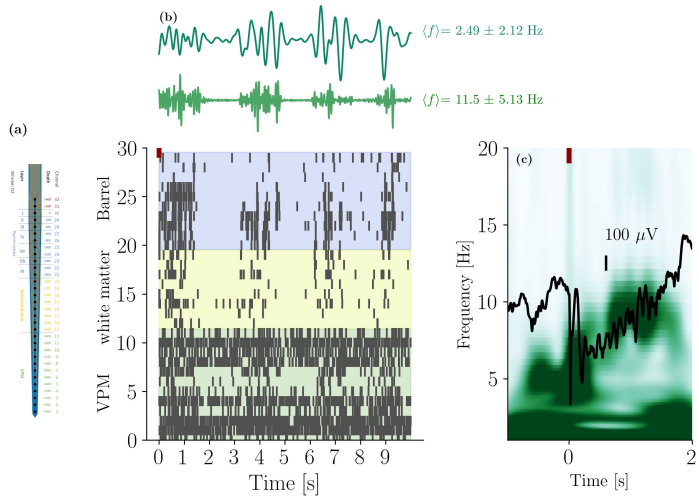

Figure 1. Experimental setup and example of the quantities that are analyzed. (a) Neural probe. The neural probe used is a 32-channel, single-shank, linear probe with a pitch between the electrodes of 200 μm. Among the total 32 channels, 30 are inserted in the brain, spanning a barrel column, a subcortical area, and part of the ventral posteromedial nucleus (VPN) of the thalamus. (b) At the bottom, an example of a 10- seconds-long raster plot (obtained by identifying events in the MUAs activity) is shown; the stimulation of the whisker is at time zero. On the top of the raster plot two main frequency components (intrinsic mode functions (IMF) 2 and 4) that contribute to the local field potentials are shown: the one with frequencies between 1 and 4 Hz and the one with frequencies between 7.5 and 15 Hz. (c) A time frequency analysis in the barrel cortex after whisker stimulation is shown, averaging over all the trials. Oscillations below 4 Hz appear during the whole recording, and oscillations centered around 11 Hz appear after the stimulation.

1 Results

Resting state neural activity in the barrel cortex and thalamus

EMD analysis of spontaneous activity oscillations

We first studied oscillations during spontaneous (resting state) activity in the barrel cortex and thalamus (see Figure 1 for the experimental setup). To characterize these oscillations during spontaneous activity we applied the empirical mode decomposition (EMD) method to the local field potentials (LFPs). This method allows for a decomposition of a signal into components that takes into account the transient and non-linear nature of physiological signals, as opposed to a decomposition into Fourier components. The components of the EMD method are called intrinsic mode functions (IMFs). We focused on the second intrinsic mode function (IMF 2) which has frequencies in the range of the whisker response (7.5–15 Hz) and the intrinsic mode function number 4 (IMF 4), which is a low-frequency oscillation with frequencies in the range 1.8–3.75 Hz. Using the Hilbert transform [67] we obtained the Hilbert spectrum, which is a weighted non-normalized joint amplitude-frequency-time distribution [30]. In particular, here we focused on the marginal spectrum (see Methods section), obtained by integrating the Hilbert spectrum over time. We thus obtained the power of the

	Rat 1	Rat 2	Rat 3	Rat 4
IMF-2 peak stim cort. vs IMF-2 peak rest cort.	pv =0.0002	pv=0.005	pv = $9e^{-8}$	pv = $1.16e^{-6}$
IMF-4 peak stim cort. vs IMF-4 peak rest cort.	pv = 0.99	pv = 0.18	pv = 0.56	pv = 0.15
IMF-2 peak stim thal. vs IMF-2 peak rest thal.	pv = 0.18	pv = 0.18	pv = 0.75	pv = 0.07
IMF-4 peak stim thal. vs IMF-4 peak rest thal.	pv = 0.98	pv = 0.2	pv = 0.76	pv = 0.1
IMF-2 peak stim cort. vs IMF-2 peak stim thal.	pv = $4e^{-6}$	pv = $2e^{-6}$	pv = $9e^{-17}$	pv = $3.8e^{-6}$
IMF-2 peak rest cort. vs IMF-2 peak rest thal.	pv = $7e^{-11}$	pv = $2e^{-6}$	pv = $9e^{-7}$	pv = $3e^{-11}$

Table 1. One-sided t-tests p-values: the peak of the marginal Hilbert spectrum of IMF 2 and IMF 4 is calculated for a barrel cortex layer IV channel (labeled as "cort." in the table) and for a central thalamus channel (labeled as "thal." in the table), in all the 30 trials, considering 2 seconds after stimulations and 2 seconds of spontaneous activity. Several tests are performed among the peak values obtained to compute paired t-tests (barrel vs barrel or thalamus vs thalamus) or unpaired t-tests (barrel vs thalamus) among the values of the spectrum peaks.

individual IMFs (for each trial) and then extracted the values of their peaks. In Figure 2 the marginal spectrum for IMF 2 and IMF 4 in all the trials is shown, both for a channel positioned in the barrel cortex (Fig. 2 a) and for a channel recording thalamus activity (Fig, 2 b). We made a statistical comparison (t-test) between the barrel cortex and the thalamus in terms of the intensity of the IMF power peaks (Table 1). We found that power of IMF 2 peaks is significantly higher in the barrel cortex as compared to the thalamus during spontaneous activity (see Figure 2).

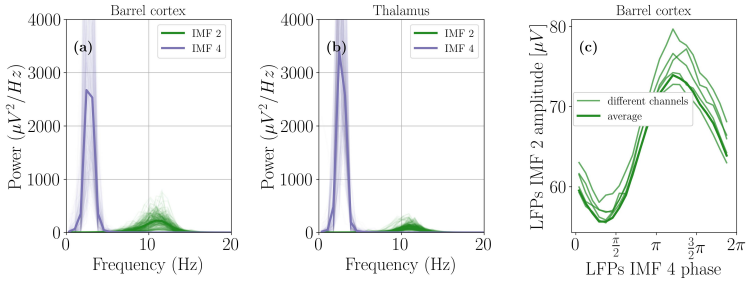

Figure 2. Barrel cortex and thalamus oscillatory activity during spontaneous activity. (a and b) Marginal Hibert spectrum of the IMF 2 and IMF 4 rhythms during the spontaneous activity of the barrel, both in the layer IV of the barrel cortex (a) and in the thalamus (b). (c) Phase amplitude coupling between the phase of IMF 4 and the amplitude of IMF 2 of the LFP signal in the barrel cortex.

Given the presence of oscillations during resting-state periods, we explored whether the slow oscillation (IMF 4, 1.8–3.75 Hz) modulates the amplitude of the faster oscillation (IMF 2, 7.5–15 Hz) via phase-amplitude coupling (PAC). As seen in Figure 2 (c), there is a sinusoidal relationship between the phase of IMF 4 and the amplitude of IMF 2, indicative of PAC and nested oscillations [5, 37, 40] within the barrel cortex.

Avalanche dynamics during spontaneous activity

We then studied the distribution of avalanches during spontaneous activity by analyzing multi-unit activity (MUA) recordings. Indeed, as opposed to LPFs, MUAs display discrete events by nature and thus allow an avalanche analysis less sensitive to signal-thresholding [42, 68, 70]. Power-law distributions were observed both in the duration and size of the avalanches, i.e., we found that the avalanches' sizes were distributed as $p(S) \sim S^{-\tau}$ and the avalanches' durations as $p(T) \sim T^{-\tau_t}$ (Figure 3 (a,

b)). Interestingly, the exponent δ linking the average size given duration $\langle S \rangle(T)$ and the duration itself of an avalanche T (see inset in Figure 3b) is $\delta = 1.31 \pm 0.04$, close to the one observed by [20, 24, 42]. We also computed avalanches' density, defined as a measure of the presence of avalanches in a given interval of time (see Figure 3 (c, d)). We computed the coupling between the slow oscillation phase and the fraction of avalanches derived from multi-unit activity (MUA), which also follows a sinusoidal pattern consistent with the one observed in LFP signals (Figure 3 (c, d)). This suggests that avalanches consistently occur in specific phases of the slow oscillation, following the same pattern of the IMF 2 oscillation (Figure 2 (c)).

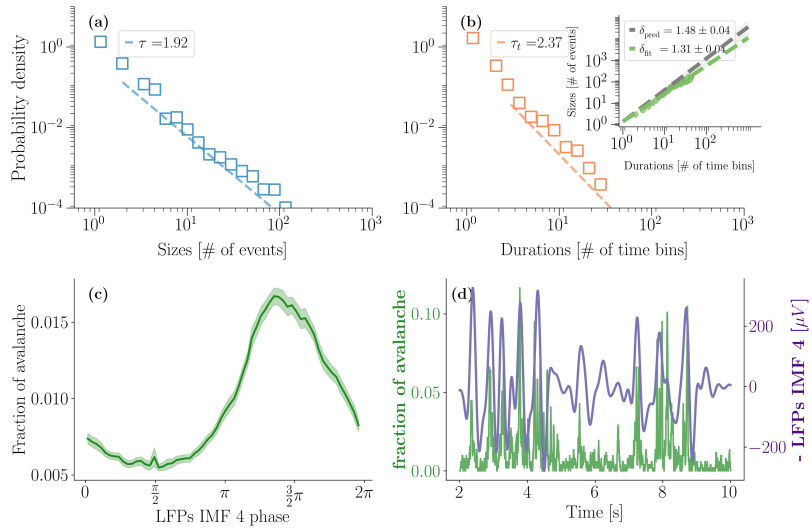

Figure 3. Avalanches during spontaneous activity and coupling between the slow oscillation and the fraction of avalanches. (a, b) Avalanches' sizes (S) (a) and durations (T) (b) distribution in the barrel cortex during spontaneous activity calculated using MUAs. In the inset of (b) it is possible to see the relation between $\langle S \rangle(T)$ and T. (c) Coupling between the phase of IMF 4, i.e. the low-frequency oscillation of the barrel signals and the fraction of avalanches. (d) Example of a trace of the fraction of avalanches with the respective evolution of IMF 4. Note that IMF 4 in Figure (d) has been flipped with respect to the $x-$axis since in local field potentials (LFPs), negative peaks correspond to neural population activations. In contrast, avalanche density is always expressed as a positive quantity and does not exhibit negative values.

Neural activity after whisker stimulation

EMD Analysis of post-stimulation oscillations

We also applied the EMD analysis in the periods following whisker stimulation, to understand its effect on IMFs 2 (7.5–15 Hz) and 4 (1.8–3.75 Hz). We again used the Hilbert-Huang transform to extract the power of the peak of each IMF considering a time interval of two seconds after the stimulation. We then performed t-tests on the IMF power peaks for statistical comparisons between the barrel cortex and the thalamus, both during rest and after stimulation intervals (Table 1). Results indicated a significant difference in the 7.5–15 Hz band (IMF 2) between spontaneous and post-stimulus activity within the barrel cortex. Whisker stimulation reinforces the oscillation in this frequency range. Moreover, as found in resting state recordings, the peaks in this band were more pronounced in the barrel cortex than in the thalamus, as shown in Figure 4. In contrast, oscillations in the 1.8–3.75 Hz band (IMF 4) were

present consistently across both cortex and thalamus without significant differences between resting and post-stimulus states.

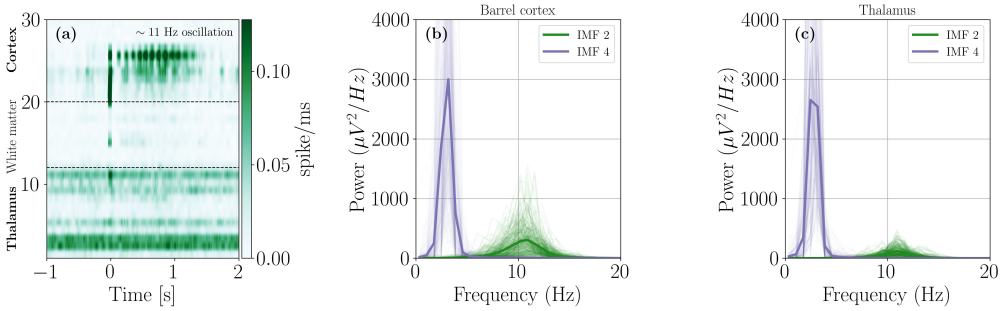

Figure 4. Barrel cortex and thalamus oscillatory activity after whisker stimulation. (a) Firing rate obtained from MUAs by averaging across all trials, after whisker stimulation (at time zero). Oscillatory activity at 11 Hz is observed in the barrel cortex immediately after stimulation. Such oscillation is absent in the thalamus. (b,c) Marginal Hilbert spectrum of IMF 2 and 4. As in the case of spontaneous activity, the power of the IMF 2 is significantly higher in the barrel than in the thalamus. Moreover, by comparing insets (b) and (c) with those of Figure 2, there is a significant increase in the power of IMF 2 after whisker stimulation (but see also Table 1).

Avalanche statistics after stimulation

After whisker stimulation, we analyzed avalanche dynamics, finding a power-law distribution in avalanche sizes, as observed during spontaneous activity (see supplementary material). However, a slight bump in the distribution was observed, corresponding to large avalanches related to the stimulus. This result is consistent with our previous finding [42]. These enhanced avalanches co-occurred with IMFs 2 (7.5–15 Hz) oscillations in the barrel cortex (Figure 4 (b)), suggesting that post-stimulation oscillations may coexist with an increase in avalanche activity.

Modelling the neural dynamics in the barrel cortex

Oscillatory activity in the model in resting state

Finally, we investigated the emerging properties of the neural dynamics of the barrel cortex by using a modified version of the reduced model proposed by Pinto and Ermentrout [50, 51] schematized in Figure 5 (a). We use the same set of parameters identified experimentally in a previous study [36], which were fitted to match the neural activity observed in the barrel cortex following whisker stimulation in rats (see Methods for details). The only exception was for the parameters that describe the cortical-thalamic connections, that were calibrated to describe our data and differ (within the experimental standard deviations provided by [50]) with those obtained in the Kyriazi and Simons study [36]. Specifically, the weight of the connection between the thalamus and the inhibitory population (w_{ti}) was decreased. In such a way, while the internal circuit of the barrel cortex remains dominated by inhibition, as was the case in the original derivation of the model [50], our model contains limit cycles in its dynamical repertoire with frequencies in the range of 10-15 Hz, remarkably close to the ones of IMF 2 that we find experimentally. Interestingly, using MUAs firing rates from the thalamus at resting state as input, the model exhibits both slow oscillations (IMF 4) and 10-15 Hz oscillations (IMF 2), that can be observed experimentally. Figure 5 (b, c)

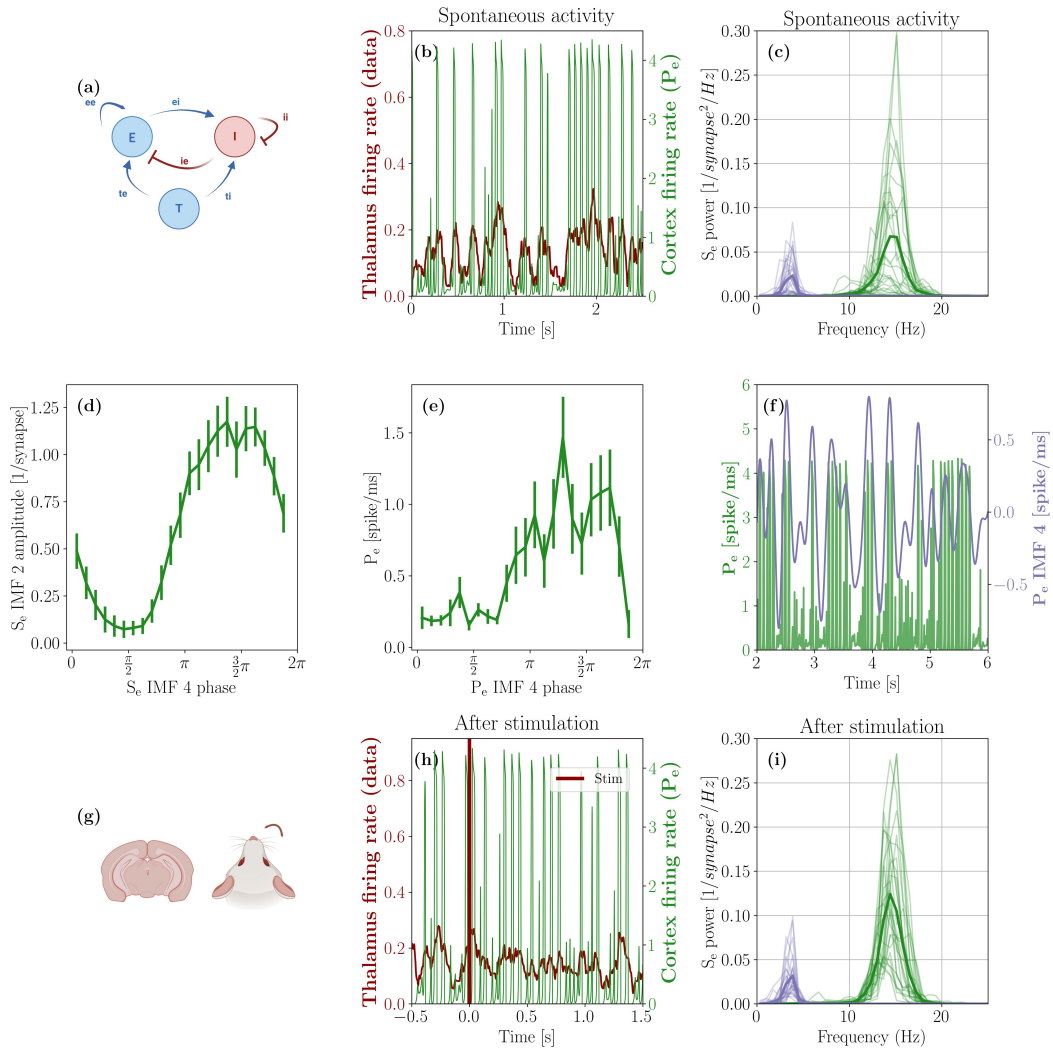

Figure 5. Modeling framework (a) Schematic illustration of the cortical barrel circuit (composed of an excitatory (E) and an inhibitory (I) subpopulation) that receives external excitatory input from the thalamus (T). (b) In red, the time histograms of the firing rate of the thalamus (P_T) during spontaneous activity obtained directly from MUAs, used as input of the model. In green, the firing rate of the excitatory units of the barrel cortex (P_e) in response to the thalamic input. (c) Marginal spectrum of the intrinsic mode functions (IMF) of the modeled cortical excitatory population. (d) Phase-amplitude coupling is computed on the simulated data, which provides the relation between the phase of the low-frequency oscillation (IMF 4) and the amplitude of the high-frequency oscillation (IMF 2); note that the phase of the IMF 4 has been shifted of π, in order to help a comparison with Figures 2 and 3) where the IMF 4 of the Local Field Potential is considered (and thus in that case negative excursion corresponds to activation of populations of neurons). (e) We also measured the coupling between the phase of IMF 4 and the firing rate in the model. This result can be compared to the avalanches in 3. (f) The firing rate in the model $\mathrm{P_e}$ and IMF 4. In (h, i) the same quantities of (b, c) are shown, yet giving as input the experimental thalamus' firing rate after a whisker stimulation, as depicted in (g).

shows the activity of the model and power spectrum for IMF 2 and IMF 4 for spontaneous activity.

Phase-amplitude coupling and avalanche dynamics in the model

We also computed the phase-amplitude coupling between the two frequencies exhibited by our model (below 4 Hz and 10-15 Hz) and found that they constitute nested oscillations, as observed in Figure 5 (d). Indeed, it shows a sinusoidal relationship between the phase of the slow oscillation and the amplitude of the faster oscillation. This is evident both by studying the coupling with the IMF 2 amplitude of S_e (Figure 5 (d)) and with the model firing rate itself P_e (Figure 5 (e,f)), which can be compared to the density of avalanches in Figure 3 (c ,d).

Model Response to Whisker Movement

We then explored the model prediction of the neural activity after whisker movement by using as input the corresponding MUAs firing rates from the thalamus. We emphasize that we did not modify any of the parameters previously used to describe the resting state (see Table 2); the only change was the thalamic input, which we replaced with the experimentally measured firing rate following whisker stimulation (see Figure 5(h)). Remarkably, the model predicts the enhancement of the 10–15 Hz oscillations (IMF 2) (see Figure 5 (i)). We then performed a statistical (t-test) analysis of the peaks of the power of the excitatory population in the model. It indicated that the power of IMF 2 is significantly higher in the after-stimulation period as compared to the resting state. This is in accordance with our experimental results of table 1.

2 Discussion

In the current study, we investigated oscillations and avalanches in the rat thalamocortical circuit, both during spontaneous activity and after mechanical stimulation of the whiskers. In both cases, a low-frequency oscillation (IMF 4, below 4 Hz) was detected concomitantly with a high frequency oscillation (IMF 2, 7.5–15 Hz). When the whisker is stimulated, the power of this oscillation increases in several layers of the barrel cortex. In the thalamus this phenomenon was not observed. In general, the power of the higher frequency oscillation was larger in the barrel cortex compared to the thalamus, both in the evoked activity and in the spontaneous activity. In contrast, the power of the low- frequency oscillation in the barrel cortex did not change after whisker stimulation. Our results show a clear phase–amplitude coupling between low- and high-frequency oscillatory activity, where the phase of the slower rhythm modulates the amplitude of faster oscillations, consistent with the concept of "nested" oscillations [5]. This is in line with prior work by Ito et al., who demonstrated modulation of gamma-band local field potential amplitudes by the respiratory rhythm [32], and with studies on the human thalamus that describe structurally constrained phase–amplitude coupling [37, 40].

We found that neuronal avalanches follow a power-law distribution, indicative of complex temporal and spatial dynamics reminiscent of criticality [15, 39]. Importantly, the phase of low-frequency oscillations modulates the density of avalanches calculated from multi-unit activity (MUA), mirroring the nesting seen in the LFPs.

Our earlier work [43] showed that critical-like dynamics, characterized by enhanced mutual information between spiking neurons across brain regions, can emerge under time-varying external inputs. In the context of the barrel cortex, thalamic inputs provide such modulatory drive. In this study, we extend those findings by showing that

thalamic input shapes both spontaneous coordination and sensory-evoked cortical responses.

We hypothesize that the "critical like" dynamics observed during resting state may provide an environment that supports the coexistence of oscillations and avalanches, allowing for a flexible, but yet structured, resting state network that may "prime" the cortex for rapid, coherent responses to whisker input. If this were the case, such preparatory dynamics could enhance the cortex's ability to integrate incoming sensory information, implying that whisker-related processing is facilitated by resting-state activity. The oscillations observed after whisker stimulation were already in the intrinsic repertoire of the resting state [11, 62] and they may set a temporal scaffold within which avalanches can propagate in response to specific sensory stimuli.

The interpretation we propose here is supported by our reduced excitatory-inhibitory neuronal population model. Indeed, by driving the model with empirical thalamic firing rates, we replicated the observed 10–15 Hz oscillations during rest and predicted their amplification upon stimulation.

Interestingly, spindle oscillations in the 7.5–15 Hz range—previously observed in barrel cortex LFPs during sleep and anesthesia [66]—share this frequency band. Spindles, known to support memory consolidation [28], have also been documented during development [33] and anesthesia [14]. While we did not perform a formal spindle detection, the analyzed frequency range likely includes spindle activity.

This rhythm has been associated with resting-state synchrony, attention modulation, sensory hypersensitivity, and even seizure-like events [19, 58, 59, 63]. Spindles are believed to originate in the thalamus [45], a hypothesis consistent with our model: oscillatory cortical output emerges when thalamic input exceeds a threshold, even though the input lacks spindle-like patterns.

Moreover, the present work contributes to show that these 7.5–15 Hz spindle-like oscillations may be a relevant collective neural activity for the processing of whisker-related sensory input in the barrel cortex, and it is important to notice that their frequency is remarkably close to the one of whisker twitching (7-12 Hz). The fact that our model admits a limit cycle in the barrel cortex has an important consequence in terms of oscillation theory. Indeed, in oscillation theory, the existence of a limit cycle or self-sustained oscillation is the basic ingredient for synchronization phenomena [49]. So, given the closeness of the frequency ranges of whisker (7-12 Hz) and barrel oscillations (7.5–15 Hz), we hypothesize that a synchronization mechanism could facilitate information transfer between these regions over a wide frequency range. Notably, we verify this hypothesis in a different work [66]. Our results thus support the hypothesis that spontaneous neural activity in the barrel cortex plays a significant physiological role, priming the barrel cortex for efficient processing of sensory input from whisker movements.

3 Methods

Surgical preparation

All experimental procedures are approved by the local Animal Care Committee (OPBA) and the Italian Ministry of Health (authorization number 522/2018-PR). Wistar rats are kept in the animal research facility of the Department of Biomedical Sciences of the University of Padua under standard environmental conditions. Young adult rats undergoing the experiments are in the range of P25-P35 (being P0 on the day of birth) with a body weight between 80 and 160 g and of both genders. Electrophysiological signals are acquired at 25 kHz from a 32 iridium-oxide electrodes array using an RHS stimulation/recording controller from Intan Technologies (Los Angeles, California,

USA). Rats are anesthetized with an intraperitoneal induction dose of urethane (0.15/100 g of the body weight), followed after half an hour by an additional dose (0.015/100 g of the body weight) [4] and after other 10 minutes by a sub-cutaneous dose of Carprofen painkiller (Rimadyl; 0.5 mg/100 g of the body weight). The animal is then positioned on a stereotaxic frame and the head is fixed by teeth- and ear-bars. Body temperature is maintained at 37°C by a heating pad and monitored by a rectal probe using a homeothermic monitoring system (World Precision Instruments ATC1000 DC temperature controller) throughout the procedure. An anterior-posterior opening in the skin is made in the center of the head and a dedicated window in the skull is drilled over the right somatosensory barrel cortex at stereotaxic coordinates from -1 to -4 AP, from $+4$ to $+8$ ML referred to as bregma [60, 65], and the probe is inserted orthogonally to the cortical surface using a micromanipulator (PatchStar; Scientifica). The depth is set at 0 when the electrode proximal to the chip tip touches the cortical surface. An Ag/AgCl electrode bathed in standard Krebs solution (in mM: NaCl 120, KCl 1.99, NaHCO 3 25.56, KH 2 PO 4 136.09, CaCl 2 2, MgSO 4 1.2, glucose 11) in proximity of the probe is used as a reference.

Electrophysiological Recordings

Thalamocortical signals are recorded by inserting a 32-channels linear probe (E32+R-200-S1-L20 NT, Atlas Neuro, Leuven, Belgium, with a pitch between the electrodes of 200 μm) at coordinates -2.9 AP, $+6.4$ ML. This allowed to acquire simultaneous signals from the barrel cortex and the ventral posteromedial nucleus (VPM) of the thalamus using 30 out of the 32 channels. Whiskers are cut to 10 mm and individually inserted up to 8 mm into a 25G hypodermic needle (BD Plastipak, Madrid, Spain), that is glued to a multilayer piezoelectric bender with integrated strain gauges and powered by a power amplifier (P-871.122 & E-650.00, Physik Instrumente, Karlsruhe, Germany). The mechanical stimulation is controlled by a waveform generator (Agilent 33250A 80 MHz, Agilent Technologies Inc., Colorado, USA), whose output is recorded synchronously with the neural signal. The most responsive whisker, i. e. the one providing the highest evoked LFP amplitude, is then selected for recording and stimulation. Data are collected in 5-minutes sets of 30 stimulation trials, while stimulations of the whisker are administered mechanically by a displacement of the cannula of 5 ms duration and 100 μs rise/fall time every 10 seconds. This long time between stimuli ensures protection against any dynamic adaptation to stimuli [14]. To extract Local Field Potentials data from the raw recording, the signals are filtered straight and reverse to achieve linear phase with a second-order bandpass Butterworth IIR filter with a cutoff frequency of 0.1 Hz (lower) and 150 Hz (higher). In the thalamocortical recordings an artifact at 100 Hz is evident, and it is eliminated in the LFPs through a notch filter. To extract multiunits activity data (MUAs) from the raw recording, the signals are filtered straight and reverse to achieve linear phase with a second-order bandpass Butterworth IIR filter with a cutoff frequency of 300 Hz (lower) and 3 kHz (higher). The spatial average of the signal recorded by the 32 channels is removed from each channel to reduce the correlated noise. [55].

Data analysis

Firing Rate

MUAs are recognized by detecting negative peaks below a threshold of 4/0.675 times the median of the absolute value of the signal [55]. The firing rate is estimated by the sum in a moving window of 60 ms of the spikes detected in each channel.

Time frequency analysis averaged across trials

We study the oscillatory response after stimulation employing standard methods based on averaging across trials the results of an event-related Fourier analysis. In particular, we applied a Morlet Wavelet analysis to the signals considering one second before whisker stimulation and two seconds after. The frequencies of the Morlet Wavelets are 50, logarithmically chosen between 1 and 25, while the parameter referring to the wavelet's number of cycles is set to 7. Then, the results for each channel are averaged across trials, in order to obtain the dynamics in power related to the whisker stimulation event.

Empirical Mode Decomposition (EMD) and intrinsic mode functions (IMF)

We use empirical mode decomposition (EMD) [30] through the EMD package [54] in order to study the frequency content of non-stationary and non-linear physiological signals. The EMD isolates a small number of temporally adaptive basis functions (intrinsic mode functions, IMF) and derives the dynamics in frequency and amplitude directly from them. The IMFs are obtained through an iterative process called sifting [30], that ensures that the EMDs are symmetric with respect to the local zero mean, and have the same numbers of zero crossings and extrema. This ensures a well-defined instantaneous frequency. Indeed, after performing the Hilbert transform [67] on each IMF component Y_j, and after computing the instantaneous frequency as $\omega_j(t) = \frac{\mathrm{d}\theta_j(t)}{\mathrm{d}t}$ (where $Y_j(t) = a_j(t)\mathrm{e}^{\mathrm{i}\theta_j(t)}$), we can express the data in the following form

$$X(t) = \sum_{j=1}^{n} a_j(t) \exp\left(\mathrm{i} \int \omega_j(t)\mathrm{d}t\right). \tag{1}$$

where the index j indicates the j-th IMF and $\omega_j(t)$ and $a_j(t)$ are respectively the instantaneous frequency and amplitude for IMF j at time t. Thus, we have broken through the restriction of the constant amplitude and fixed-frequency Fourier expansion, and arrived at a variable amplitude and frequency representation.

Equation 1 also enables us to represent the amplitude and the instantaneous frequency as functions of time in a three-dimensional plot, in which the amplitude can be contoured on the frequency-time plane. This frequency-time distribution of the amplitude is designated as the Hilbert amplitude spectrum, $H(\omega, t)$, or simply Hilbert spectrum. In particular, in this work, we have considered the marginal Hilbert Spectrum,

$$h(\omega) = \int_0^T H(\omega, t)\mathrm{d}t.$$

The marginal spectrum offers a measure of total amplitude (or energy) contribution from each frequency value. The frequency in either $H(\omega; t)$ or $h(\omega)$ has a totally different meaning from the Fourier spectral analysis. In the Fourier representation, the existence of energy at a frequency, ω, means a component of a sine or a cosine wave persisted. through the time span of the data. Here, the existence of energy at the frequency, ω, means only that, in the whole time span of the data, there is a higher likelihood for such a wave to have appeared locally. In fact, the Hilbert spectrum is a weighted non-normalized joint amplitude-frequency-time distribution.

To a correct application of the EMD algorithm, common practice states that the IMFs should be well separated - the components should have low correlations/orthogonality scores - and the instantaneous frequency content of the IMFs should not strongly overlap (no mode mixing). This can be achieved by using a pseudo-mode splitting index (PMSI) [17]. In particular, we applied to the local field potential recordings a mask-sift algorithm, that overcomes some limitations of the

standard sift algorithm with intermittent and noisy signals [12], by masking some chosen frequencies in the signals so to avoid mode mixing. Indeed, choosing a frequency mask effectively puts a lower bound on the frequency content that can enter a particular IMF. The frequency of the first mask was set to 30 Hz, and the mask step factor was set to 2 (default value) [54] (by simulations, it was shown that a mask at a given frequency f suppresses frequencies below $0.7 \times f$ [22]).

Phase amplitude coupling

Phase amplitude coupling is computed by using the EMD package [54] between the second IMF amplitude and the fourth IMF phase. Cycles are detected in the fourth IMF, and the corresponding phase is binned. Then, the amplitude of IMF 2 is associated with its respective phase bin, and the amplitude values are averaged across all the cycles that are found.

Avalanches' statistics and avalanches' density

Avalanches are computed using standardized pipelines [3, 42]. MUAs are recognized by detecting negative peaks below a threshold of 3/0.675 times the median of the absolute value of the signal. Then, the average inter-event interval is computed [3] to bin the data, and avalanches are detected as sequences of time bins with activity, separated by empty bins. The number of events in an avalanche is the size of an avalanche, while the number of bins is the duration of an avalanche. They are fitted with power-laws using a corrected maximum-likelihood method [42]. Indeed, the avalanches sizes and durations distributions are fitted using the maximum likelihood method. The fitting function for both avalanche sizes and duration is a discrete power-law:

$$p(y;\alpha) = \frac{y^{-\alpha}}{\sum_{x=x_{min}}^{x=x_{max}} x^{-\alpha}}. \tag{2}$$

The parameter x_{max} is set to the maximum observed size or duration. Then the tails of the distributions are fitted by selecting as parameter x_{min} the one that minimizes the Kolmogorov-Smirnov distance (KS), following the method proposed by Clauset et al. [10]:

$$\mathrm{KS} = \max_{y \geq x_{min}} |S(y) - \hat{P}(y)| \tag{3}$$

where $S(y)$ is the cumulative distribution function (CDF) of the data and $\hat{P}(y)$ is the CDF of the theoretical distribution fitted with the parameter that best fits the data for $y \geq x_{min}$.

After finding the best-fit power law, to assess goodness-of-fit we compared the experimental data against 1000 surrogate datasets drawn from the best-fit power law distribution with the same number of samples as the experimental dataset. The deviation between the surrogate datasets and a perfect power law was quantified with the KS statistic. The p-value of the power-law fit was defined as the fraction of these surrogate KS statistics which were greater than the KS statistic for the experimental data. Note that the data were considered power law distributed if the null hypothesis could not be rejected, namely if the the p-value turned out to be greater than the significance level, which was set to a conservative value of 0.1.

Then, the avalanche density as a function of time is calculated, as it was proposed in [57], i.e., the fraction of time occupied by avalanches in a time T_0, with a sliding step of $t = \frac{1}{\text{sampling rate}}$. T_0 was set to $5 \times$ average inter event interval.

Table 2

parameter	symbol	value
resting potential (mv)	ρ	-60 mV
firing threshold (mv)	θ	-45 mV
temperature	T_e	12.03
-	T_i	11.62
conversion factor	γ_e	5
-	γ_i	15
refractory parameter	e_r	2.2
-	i_r	4.1
connection strength (mv)	w_{ee}	1.0
-	w_{ei}	1.0
-	w_{ie}	2.0
-	w_{ii}	1.5
-	w_{te}	3.9
-	w_{ti}	1.5
number of synapses	ec	42
-	ic	12
-	tc_e	12
-	tc_i	10
decay constant (ms)	τ_e	5
-	τ_i	15

Reduced model of the barrel cortex

Brain activity in the barrel cortex was modeled using a set of equations similar to the well-known Wilson-Cowan system [74]. This model has been previously used to describe the barrel cortex of rats, providing a good qualitative and quantitative agreement with anatomical and physiological properties of the barrel cortex as well as its response to whisker stimulation [50]. This model is the result of a reduction of a biologically detailed spike-model of a single barrel previously developed by Kyriazi and Simons [36] (with 70 excitatory and 30 inhibitory neurons, modeled as leaky linear integrators). The resulting model consists of one excitatory and one inhibitory neuronal population simulating the barrel cortex, connected with each other and receiving thalamic input. The thalamic input is introduced in the form of time histograms (TH). The corresponding equations describe the dynamics of the average synaptic drive of both excitatory and inhibitory populations,

$$\begin{aligned}
\tau_e \frac{dS^e}{dt} &= -S_e(t) + \gamma_e(1 - erP_e(S_e))P_e(w_{ee}ecS_e(t) + w_{te}tc_eS^T(t) - w_{ie}icS^i(t)) \\
\tau_i \frac{dS^i}{dt} &= -S_i(t) + \gamma_i(1 - irP_i(S_i))P_i(w_{ei}ecS_e(t) + w_{ti}tc_iS^T(t) - w_{ii}icS^i(t)) \\
\tau_e \frac{dS^T}{dt} &= -S_T(t) + TH(t),
\end{aligned}$$

The reduced equations succinctly define the relationship between three distinct measures of neuronal activity (see equation 4, in which for simplicity we don't consider the refractory effect), as mentioned in the main text: voltage, firing rate, and a measure which we describe as synaptic drive (S_e and S_i are the synaptic drives and are linked to the firing rate through the conversion factors γ_e, γ_i of the excitatory and inhibitory

populations, respectively).

$$\tau_e \frac{dS^E}{dt} + \underbrace{S^E(t)}_{\text{Synaptic Drive}} = \overbrace{P_e(\underbrace{w_{ee}ecS^E(t) + w_{te}tcS^T(t) - w_{ie}icS^I(t)}_{\text{Voltage}})}^{\text{Firing rate}} \tag{4}$$

P_e and P_i are activation functions (excitatory and inhibitory), given by,

$$P_{e,i}(V) = \frac{1}{2}\left(1 + erf\left(\frac{V - (\theta - \rho)}{T_{e,i}}\right)\right), \tag{5}$$

where V is the membrane potential and $T_{e,i}$ is the temperature for activation function of the excitatory and inhibitory populations. The parameters θ and ρ are the firing threshold and the resting membrane potential, respectively. Here $erf(x)$ is the Gauss error function, defined in the usual way,

$$erf(x) = \frac{2}{\sqrt{\pi}} \int_0^x e^{-y^2} dy. \tag{6}$$

The parameters of the model used in this work are summarized in table 2 and were calibrated experimentally [36].

In our case, we give as input to the model the time histograms of thalamus activity either after stimulation of the rat whisker or during spontaneous activity. Note that the balance of feedforward (thalamic) inhibition over excitation ($\frac{w_{ti}}{w_{te}}$) and the refractory parameter er are varied (see Table 2, but within the standard deviations provided by [36]) so that the model can admit a limit cycle and behaves as an amplifier, as predicted in [51] (while it behaves as a damper with higher values of w_{ti}).

4 Author contributions

S.S. and S.V. conceived the study and were in charge of overall direction and planning. M.M., and A.L. carried out the experiments. R.G., B.M., and S.S. designed the theoretical framework. B. M. analyzed the data and M. T. provided guidance in the data analysis. B.M. and R.G. planned the simulations and B. M. carried out and analyzed the simulations. All authors contributed to the interpretation of the results, provided critical feedback, and helped shape the research, analysis, and manuscript.

5 Acknowledgments

Work by S.S. and B.M. is supported by NEXTGENERATIONEU (NGEU) and funded by the Ministry of University and Research (MUR), National Recovery and Resilience Plan (NRRP), project MNESYS (PE0000006) – A Multiscale integrated approach to the study of the nervous system in health and disease (DN. 1553 11.10.2022). The funders had no role in study design, data collection and analysis, decision to publish, or preparation of the manuscript.

References

1. Y. Ahmadian and K. D. Miller. What is the dynamical regime of cerebral cortex? *Neuron*, 109(21):3373–3391, 2021.

2. G. Barzon, G. Nicoletti, B. Mariani, M. Formentin, and S. Suweis. Criticality and network structure drive emergent oscillations in a stochastic whole-brain model. *Journal of Physics: Complexity*, 3(2):025010, 2022.

3. J. M. Beggs and D. Plenz. Neuronal avalanches in neocortical circuits. *Journal of Neuroscience*, 12:23(35):11167–11177, 2003.

4. G. J. Benson, J. C. Thurmon, and W. J. Tranquilli. *Lumb & Jones' Veterinary Anesthesia*. Lippincott Williams & Wilkins, 1996.

5. M. Bonnefond, S. Kastner, and O. Jensen. Communication between brain areas based on nested oscillations. *eneuro*, 4(2), 2017.

6. G. Buzsaki. *Rhythms of the Brain*. Oxford University Press, 2006.

7. G. Buzsáki, N. Logothetis, and W. Singer. Scaling brain size, keeping timing: evolutionary preservation of brain rhythms. *Neuron*, 80(3):751–764, 2013.

8. R. L. Carhart-Harris, R. Leech, P. J. Hellyer, M. Shanahan, A. Feilding, E. Tagliazucchi, D. R. Chialvo, and D. Nutt. The entropic brain: a theory of conscious states informed by neuroimaging research with psychedelic drugs. *Frontiers in human neuroscience*, 8:55875, 2014.

9. D. R. Chialvo. Emergent complex neural dynamics. *Nature physics*, 6(10):744–750, 2010.

10. A. Clauset, C. R. Shalizi, and M. E. Newman. Power-law distributions in empirical data. *SIAM review*, 51(4):661–703, 2009.

11. G. Deco, V. K. Jirsa, and A. R. McIntosh. Emerging concepts for the dynamical organization of resting-state activity in the brain. *Nature reviews neuroscience*, 12(1):43–56, 2011.

12. R. Deering and J. F. Kaiser. The use of a masking signal to improve empirical mode decomposition. In *Proceedings.(ICASSP'05). IEEE International Conference on Acoustics, Speech, and Signal Processing, 2005.*, volume 4, pages iv–485. IEEE, 2005.

13. D. Derdikman, R. Hildesheim, E. Ahissar, A. Arieli, and A. Grinvald. Imaging spatiotemporal dynamics of surround inhibition in the barrels somatosensory cortex. *Journal of Neuroscience*, 23(8):3100–3105, 2003.

14. D. Derdikman, C. Yu, S. Haidarliu, K. Bagdasarian, A. Arieli, and E. Ahissar. Layer-specific touch-dependent facilitation and depression in the somatosensory cortex during active whisking. *Journal of Neuroscience*, 26(37):9538–9547, 2006.

15. S. Di Santo, P. Villegas, R. Burioni, and M. A. Muñoz. Landau–ginzburg theory of cortex dynamics: Scale-free avalanches emerge at the edge of synchronization. *Proceedings of the National Academy of Sciences*, 115(7):E1356–E1365, 2018.

16. M. E. Diamond, M. Von Heimendahl, P. M. Knutsen, D. Kleinfeld, and E. Ahissar. 'where'and'what'in the whisker sensorimotor system. *Nature Reviews Neuroscience*, 9(8):601–612, 2008.

17. M. S. Fabus, A. J. Quinn, C. E. Warnaby, and M. W. Woolrich. Automatic decomposition of electrophysiological data into distinct nonsinusoidal oscillatory modes. *Journal of Neurophysiology*, 126(5):1670–1684, 2021. PMID: 34614377.

18. E. E. Fanselow and M. A. Nicolelis. Behavioral modulation of tactile responses in the rat somatosensory system. *Journal of neuroscience*, 19(17):7603–7616, 1999.

19. E. E. Fanselow, K. Sameshima, L. A. Baccala, and M. A. Nicolelis. Thalamic bursting in rats during different awake behavioral states. *Proceedings of the National Academy of Sciences*, 98(26):15330–15335, 2001.

20. A. J. Fontenele, N. A. P. de Vasconcelos, T. Feliciano, L. A. A. Aguiar, C. Soares-Cunha, B. Coimbra, L. Dalla Porta, S. Ribeiro, A. J. a. Rodrigues, N. Sousa, P. V. Carelli, and M. Copelli. Criticality between cortical states. *Phys. Rev. Lett.*, 122:208101, 2019.

21. L. Fontolan, B. Morillon, C. Liegeois-Chauvel, and A.-L. Giraud. The contribution of frequency-specific activity to hierarchical information processing in the human auditory cortex. *Nature communications*, 5(1):4694, 2014.

22. O. B. Fosso and M. Molinas. Method for mode mixing separation in empirical mode decomposition. *arXiv preprint arXiv:1709.05547*, 2017.

23. D. Fraiman and D. R. Chialvo. What kind of noise is brain noise: anomalous scaling behavior of the resting brain activity fluctuations. *Frontiers in physiology*, 3:307, 2012.

24. N. Friedman, S. Ito, B. A. Brinkman, M. Shimono, R. L. DeVille, K. A. Dahmen, J. M. Beggs, and T. C. Butler. Universal critical dynamics in high resolution neuronal avalanche data. *Physical review letters*, 108(20):208102, 2012.

25. P. Fries. A mechanism for cognitive dynamics: neuronal communication through neuronal coherence. *Trends in cognitive sciences*, 9(10):474–480, 2005.

26. E. D. Gireesh and D. Plenz. Neuronal avalanches organize as nested theta-and beta/gamma-oscillations during development of cortical layer 2/3. *Proceedings of the National Academy of Sciences*, 105(21):7576–7581, 2008.

27. J. J. Harris, R. Jolivet, and D. Attwell. Synaptic energy use and supply. *Neuron*, 75(5):762–777, 2012.

28. R. F. Helfrich, B. A. Mander, W. J. Jagust, R. T. Knight, and M. P. Walker. Old brains come uncoupled in sleep: Slow wave-spindle synchrony, brain atrophy, and forgetting. *Neuron*, 97, 2018.

29. J. Hidalgo, J. Grilli, S. Suweis, M. A. Munoz, J. R. Banavar, and A. Maritan. Information-based fitness and the emergence of criticality in living systems. *Proceedings of the National Academy of Sciences*, 111(28):10095–10100, 2014.

30. N. E. Huang, Z. Shen, S. R. Long, M. C. Wu, H. H. Shih, Q. Zheng, N.-C. Yen, C. C. Tung, and H. H. Liu. The empirical mode decomposition and the hilbert spectrum for nonlinear and non-stationary time series analysis. *Proceedings of the Royal Society of London. Series A: mathematical, physical and engineering sciences*, 454(1971):903–995, 1998.

31. A. Hyafil, A.-L. Giraud, L. Fontolan, and B. Gutkin. Neural cross-frequency coupling: connecting architectures, mechanisms, and functions. *Trends in neurosciences*, 38(11):725–740, 2015.

32. J. Ito, S. Roy, Y. Liu, Y. Cao, M. Fletcher, L. Lu, J. Boughter, S. Grün, and D. Heck. Whisker barrel cortex delta oscillations and gamma power in the awake mouse are linked to respiration. *Nature communications*, 5(1):3572, 2014.

33. R. Khazipov, A. Sirota, X. Leinekugel, G. L. Holmes, Y. Ben-Ari, and G. Buzsáki. Early motor activity drives spindle bursts in the developing somatosensory cortex. *Nature*, 432(7018):758–761, 2004.

34. D. Kleinfeld, E. Ahissar, and M. E. Diamond. Active sensation: insights from the rodent vibrissa sensorimotor system. *Current opinion in neurobiology*, 16(4):435–444, 2006.

35. N. Kopell. We got rhythm: Dynamical systems of the nervous system. *Notices of the AMS*, 47(1):6–16, 2000.

36. H. T. Kyriazi and D. J. Simons. Thalamocortical response transformations in simulated whisker barrels. *Journal of Neuroscience*, 13(4):1601–1615, 1993.

37. P. Lakatos, A. S. Shah, K. H. Knuth, I. Ulbert, G. Karmos, and C. E. Schroeder. An oscillatory hierarchy controlling neuronal excitability and stimulus processing in the auditory cortex. *Journal of neurophysiology*, 94(3):1904–1911, 2005.

38. F. Lombardi, H. J. Herrmann, D. Plenz, and L. De Arcangelis. On the temporal organization of neuronal avalanches. *Frontiers in systems neuroscience*, 8:204, 2014.

39. F. Lombardi, S. Pepić, O. Shriki, G. Tkačik, and D. De Martino. Statistical modeling of adaptive neural networks explains co-existence of avalanches and oscillations in resting human brain. *Nature Computational Science*, 3, 2023.

40. M. Malekmohammadi, W. J. Elias, and N. Pouratian. Human Thalamus Regulates Cortical Activity via Spatially Specific and Structurally Constrained Phase-Amplitude Coupling. *Cerebral Cortex*, 25(6):1618–1628, 01 2014.

41. D. Mantini, M. G. Perrucci, C. Del Gratta, G. L. Romani, and M. Corbetta. Electrophysiological signatures of resting state networks in the human brain. *Proceedings of the National Academy of Sciences*, 104(32):13170–13175, 2007.

42. B. Mariani, G. Nicoletti, M. Bisio, M. Maschietto, R. Oboe, A. Leparulo, S. Suweis, and S. Vassanelli. Neuronal avalanches across the rat somatosensory barrel cortex and the effect of single whisker stimulation. *Frontiers in Systems Neuroscience*, 15:89, 2021.

43. B. Mariani, G. Nicoletti, M. Bisio, M. Maschietto, S. Vassanelli, and S. Suweis. Disentangling the critical signatures of neural activity. *Scientific reports*, 12(1):10770, 2022.

44. M. A. Munoz. Colloquium: Criticality and dynamical scaling in living systems. *Reviews of Modern Physics*, 90(3):031001, 2018.

45. G. T. Neske. The slow oscillation in cortical and thalamic networks: mechanisms and functions. *Frontiers in neural circuits*, 9:88, 2016.

46. T. Petermann, T. C. Thiagarajan, M. A. Lebedev, M. A. Nicolelis, D. R. Chialvo, and D. Plenz. Spontaneous cortical activity in awake monkeys composed of neuronal avalanches. *Proceedings of the National Academy of Sciences*, 106(37):15921–15926, 2009.

47. C. C. Petersen. The functional organization of the barrel cortex. *Neuron*, 56(2):339–355, 2007.

48. G. Pezzulo, M. Zorzi, and M. Corbetta. The secret life of predictive brains: what's spontaneous activity for? *Trends in cognitive sciences*, 25(9):730–743, 2021.

49. A. Pikovsky, M. Rosenblum, and J. Kurths. Synchronization: a universal concept in nonlinear science, 2002.

50. D. J. Pinto, J. C. Brumberg, D. J. Simons, G. B. Ermentrout, and R. Traub. A quantitative population model of whisker barrels: re-examining the wilson-cowan equations. *Journal of computational neuroscience*, 3:247–264, 1996.

51. D. J. Pinto, J. A. Hartings, J. C. Brumberg, and D. J. Simons. Cortical damping: analysis of thalamocortical response transformations in rodent barrel cortex. *Cerebral cortex*, 13(1):33–44, 2003.

52. S.-S. Poil, R. Hardstone, H. D. Mansvelder, and K. Linkenkaer-Hansen. Critical-state dynamics of avalanches and oscillations jointly emerge from balanced excitation/inhibition in neuronal networks. *Journal of Neuroscience*, 32(29):9817–9823, 2012.

53. A. Ponce-Alvarez, G. Deco, P. Hagmann, G. L. Romani, D. Mantini, and M. Corbetta. Resting-state temporal synchronization networks emerge from connectivity topology and heterogeneity. *PLoS computational biology*, 11(2):e1004100, 2015.

54. A. J. Quinn, V. Lopes-dos Santos, D. Dupret, A. C. Nobre, and M. W. Woolrich. Emd: Empirical mode decomposition and hilbert-huang spectral analyses in python. *Journal of Open Source Software*, 6(59):2977, 2021.

55. R. Q. Quiroga, Z. Nadasdy, and Y. Ben-Shaul. Unsupervised Spike Detection and Sorting with Wavelets and Superparamagnetic Clustering. *Neural Computation*, 16(8):1661–1687, 08 2004.

56. M. E. Raichle. The restless brain. *Brain connectivity*, 1(1):3–12, 2011.

57. S. Scarpetta, N. Morisi, C. Mutti, N. Azzi, I. Trippi, R. Ciliento, I. Apicella, G. Messuti, M. Angiolelli, F. Lombardi, et al. Criticality of neuronal avalanches in human sleep and their relationship with sleep macro-and micro-architecture. *Iscience*, 26(10), 2023.

58. K. Semba, H. Szechtman, and B. R. Komisaruk. Synchrony among rhythmical facial tremor, neocortical 'alpha'waves, and thalamic non-sensory neuronal bursts in intact awake rats. *Brain research*, 195(2):281–298, 1980.

59. F.-Z. Shaw. Is spontaneous high-voltage rhythmic spike discharge in long evans rats an absence-like seizure activity? *Journal of neurophysiology*, 91(1):63–77, 2004.

60. S. Shimegi, T. Akasaki, T. Ichikawa, and H. Sato. Physiological and anatomical organization of multiwhisker response interactions in the barrel cortex of rats. *J. Neurosci.*, 20(16):6241–6248, Aug. 2000.

61. W. Singer. Neuronal oscillations: unavoidable and useful? *European Journal of Neuroscience*, 48(7):2389–2398, 2018.

62. S. M. Smith, P. T. Fox, K. L. Miller, D. C. Glahn, P. M. Fox, C. E. Mackay, N. Filippini, K. E. Watkins, R. Toro, A. R. Laird, et al. Correspondence of the brain's functional architecture during activation and rest. *Proceedings of the national academy of sciences*, 106(31):13040–13045, 2009.

63. A. Sobolewski, D. A. Swiejkowski, A. Wróbel, and E. Kublik. The 5–12 hz oscillations in the barrel cortex of awake rats–sustained attention during behavioral idling? *Clinical Neurophysiology*, 122(3):483–489, 2011.

64. C. Stringer, M. Pachitariu, N. Steinmetz, C. B. Reddy, M. Carandini, and K. D. Harris. Spontaneous behaviors drive multidimensional, brainwide activity. *Science*, 364(6437):eaav7893, 2019.

65. L. W. Swanson. Brain maps 4.0-structure of the rat brain: An open access atlas with global nervous system nomenclature ontology and flatmaps. *J. Comp. Neurol.*, 526(6):935–943, Apr. 2018.

66. M. Tambaro, R. Guevara, M. Maschietto, A. L. Leparulo, C. Cecchetto, G. Nicoletti, B. Mariani, S. Suweis, and V. Stefano. The somatosensory barrel cortex controls the spindle thalamocortical oscillation by frequency locking. *biorXiv*, 2025.

67. E. C. Titchmarsh. *Introduction to the theory of Fourier integral.* The Clarendon Press, 1937.

68. J. Touboul and A. Destexhe. Can power-law scaling and neuronal avalanches arise from stochastic dynamics? *PLOS ONE*, 5(2):1–14, 02 2010.

69. S. Venkatraman and J. M. Carmena. Behavioral modulation of stimulus-evoked oscillations in barrel cortex of alert rats. *Frontiers in integrative neuroscience*, page 10, 2009.

70. P. Villegas, S. di Santo, R. Burioni, and M. A. Muñoz. Time-series thresholding and the definition of avalanche size. *Phys. Rev. E*, 100:012133, Jul 2019.

71. J. L. Vincent, G. H. Patel, M. D. Fox, A. Z. Snyder, J. T. Baker, D. C. Van Essen, J. M. Zempel, L. H. Snyder, M. Corbetta, and M. E. Raichle. Intrinsic functional architecture in the anaesthetized monkey brain. *Nature*, 447(7140):83–86, 2007.

72. S. B. Vincent. *The Functions of the Vibrissae in the Behavior of the White Rat...*, volume 1. University of Chicago, 1912.

73. T. Volpi, E. Silvestri, M. Aiello, J. J. Lee, A. G. Vlassenko, M. S. Goyal, M. Corbetta, and A. Bertoldo. The brain's "dark energy" puzzle: How strongly is glucose metabolism linked to resting-state brain activity? *Journal of Cerebral Blood Flow & Metabolism*, page 0271678X241237974, 2024.

74. H. R. Wilson and J. D. Cowan. Excitatory and inhibitory interactions in localized populations of model neurons. *Biophysical journal*, 12(1):1–24, 1972.

75. T. A. Woolsey and H. Van der Loos. The structural organization of layer iv in the somatosensory region (si) of mouse cerebral cortex: the description of a cortical field composed of discrete cytoarchitectonic units. *Brain research*, 17(2):205–242, 1970.